Pinning-depinning transition in dislocation dynamics

D. C. Chrzan
Department of Materials Science and Mineral Engineering, University of California, Berkeley, California 94720 and Materials Sciences Division, Lawrence Berkeley Laboratory, Berkeley, California 94720

Murray S. Daw
Department of Physics and Astronomy, Clemson University, Clemson, South Carolina 29634
(Received 25 July 1996)

We present a series of models used to analyze the motion of dislocations in $L1_2$ intermetallic compounds, which show a yield strength anomaly (increasing strength with increasing temperature). The models are presented in terms of stochastic, finite difference equations of motion and are based on physical arguments from previous work. The solutions show that the models display a pinning-depinning transition with increasing stress. The pinned phase is shown to have a large number of possible configurations. A set of deterministic, mean-field equations are derived from the stochastic equations, and used to analyze some of the statistical properties of the models. We also examine numerical solutions to the stochastic equations, and analyze them for critical exponents and scaling. Finite-size effects are likely to be very important in the practical application of these models. [S0163-1829(97)07001-X]

I. INTRODUCTION

It is agreed generally that the noncompact core structure of the $a\langle 110\rangle$ superdislocations is the origin of the yield strength anomaly observed in many $L1_2$ intermetallic compounds.[1] In particular, it is known that these dislocation cores can exist in at least two types of states: (1) a glissile state, in which all partial dislocations lie on a single $\{111\}$ plane, and (2) a sessile state, in which the partial dislocations lie on separate $\{111\}$ planes. Paidar, Pope, and Vitek analyzed the dynamic process by which a localized segment of superdislocation may convert from the glissile to a sessile state.[1] They found that the key step is a thermally activated cross-slip event. Hence, as the temperature increases, the number of localized sessile segments increases, leading to an increased drag on the motion of the dislocations. This increased drag was argued to be the origin of the anomaly, and a quantitative theory of the anomaly, based on the properties of a periodic arrangement of sessile segments, was developed.

Recently, the dynamics of the cross-slip pinning process have been incorporated into a dynamical simulation of dislocation motion.[2] Several important insights are obtained from these simulations. First, the observed superdislocation structures, consisting of long pinned segments, the so-called ''Kear-Wilsdorf locks,''[3] connected by large, potentially glissile segments of mixed character, referred to as ''superkinks,''[4–7] arise naturally from the dynamics of dislocation motion. Second, it is also noted that the dislocations of predominantly screw character advance through the lateral motion of the superkinks. Third, the superkink population along any particular dislocation fluctuates, due to primarily three processes: (1) Superkinks scatter off other superkinks resulting in annihilation of one or more superkinks. (2) Superkinks spawn new superkinks. (3) Superkinks leave the crystal through its surface.

The most important observation, however, is that the dislocations undergo a stress-driven pinning-depinning transition.[8,9] At low stresses, the dynamics of dislocation motion are such that dislocations become pinned completely (i.e., over their entire length) by numerous cross-slip events. For stresses above a critical stress, τ_c, the dislocations remain mobile for a time limited only by the finite size of the dislocation: an infinite length dislocation remains mobile for all time. The transition appears to occur abruptly at τ_c.

To study this transition, a discrete model (henceforth referred to as the ''prior model'') with dynamics constructed to mimic the dislocation dynamics observed in the continuum simulations, was developed. The scaling properties of the transition were explored, and the results were used to develop a theory of the creep properties of these compounds.[9,10]

In the pinned phase, a small increment in the stress will cause pinned segments to mobilize and sweep out an area before eventually being pinned again. The time scale for the primary creep transient is set by the time characterizing the decay of these events. In addition, these events display scaling behavior near the critical stress.

This scaling theory, while promising, leaves open questions.[9,10] One concern involves the effects of finite size on the dislocations. For example, if one assumes that each site of the segment in the prior model corresponds to a length of dislocation of the order of magnitude of the Burgers vector, i.e., approximately 5 Å, then a dislocation of length 10^{-3} m is represented by a model containing approximately 10^7 sites. Hence one may expect the effects of finite size to be relevant to experiments.

Another, and perhaps the more notable, concern involves the overall time scale of the pinning process. Results from the model indicate that expected time scales over which the scaling behavior should be observed are too short to be consistent with experimental observations. It was suggested in Ref. 10 that the addition of a thermally activated step in the dynamics of dislocation motion may correct the time-scale

 © 1997 The American Physical Society

difficulty, while preserving the scaling behavior. The original model was modified, and the effects of a thermally activated step on the overall dynamics investigated in a preliminary fashion. This model proved computationally too expensive for complete study, and many open questions remain.

In the current paper, the scaling properties of the thermally assisted pinning-depinning transition are studied more thoroughly. The prior model is simplified, and extended to a class of models. These models are studied by analytic means, within mean-field approximation, and through exact numerical simulation.

It is shown that the behavior of the models presented below is similar to that observed in the prior model of flow.[8,9] It is also shown that introduction of thermal depinning, while smearing out the pinning-depinning transition does *not* eliminate all scaling behavior. The remaining vestiges of the scaling behavior are used as a means to deduce, based on numerical results, the value of some of the exponents associated with the pinning-depinning transition in the absence of thermal depinning.

The remainder of this paper is organized as follows. The next section introduces the simplified class of models. Section III presents the exact solution to the simplest model in the class. In Sec. IV, we describe a mean-field treatment of the more complicated models. Section V presents numerical results for comparison with the mean-field analysis. We discuss the importance of various aspects in Sec. VI and conclude with Sec. VII.

II. MODELING OF DISLOCATION DYNAMICS

The models studied here attempt to capture three fundamental aspects of dislocation dynamics. The first is the cross-slip event, which happens with a probability q measured as a number of cross-slip events per unit dislocation length per unit dislocation advancement. A cross-slipped node is immobilized. The second is the athermal stress-driven mobilization of a cross-slipped segment, which occurs when mobile segments of the dislocation advance beyond and pull loose a locked segment. The third is the mobilization of a cross-slipped segment via a thermally activated process occurring with probability ε.

When cross slip fails to occur (as will happen with probability $p=1-q$), it will be seen below that superkinks can be nucleated. For example, a mobile kink can nucleate another kink at the rate p. It is expected generally that $\varepsilon \ll p$.

The origins of the parameter q warrant discussion. The cross-slip probability per unit length of dislocation per unit distance advanced decreases monotonically (and potentially nonlinearly) with the applied stress (at fixed temperature). (If this were not the case, one would expect *less* slip at *higher* stresses.) A more detailed relationship between the applied stress and cross-slip rate has *not* been developed, and remains a topic for future research. For simplicity, it is assumed that $q=q(\tau,T)$, with τ the applied stress and T the temperature, and that q is a monotonically decreasing function of the stress at fixed T. (Note that in this work it is assumed that q is independent of configuration, in contrast to the prior model, where there was some dependence of the rates on specific configuration. The current investigations indicate that the results cited are not sensitive to this difference.)

In the models developed here, a dislocation is described by a discrete set of points which can move in the direction perpendicular to the average line direction. The position in the line is denoted by the index m, and the distance moved perpendicular to the line direction is $y[m]$. Between each pair of points we define a slope, $s[m] \equiv y[m+1]-y[m]$. In the models studied here, the slopes $s[m]$ are also discrete. The dynamics of dissolution of the Kear-Wilsdorf locks dictates that the slope cannot exceed a maximum value. The number of allowed values for the slope determines the degrees of freedom of the dislocation and its behavior under an applied stress.

The models can be classified according to the allowed slopes. The simplest model considered here allows slopes of $-1/2$ and $+1/2$ and is referred to as $B(1/2)$. The next model in the sequence $B(1)$ allows the slopes to be -1, 0, or 1. In general, $B(M)$ allows the $(2M+1)$ values $-M,-(M-1),\ldots,(M-1),M$. The allowed dislocations configurations are then described in complete analogy to a one dimensional chain of spins, and $B(M)$ corresponds in this sense to a spin-M chain.

Because the state of the dislocation is given in terms of the values of $y[m]$, the dynamics of the dislocation is defined by rules governing the evolution of the $y[m]$. These rules are based on the fundamental processes. Let $y[m,i]$ to be the value of $y[m]$ at step i. The rules which give the motion of the points (i.e., the $y[m,i+1]$ from the $y[m,i]$) are based on the values of the pair of slopes which neighbor the site m (that is, $s[m-1,i]$ and $s[m,i]$). For convenience, these *slope pairs* are referred to as (s_l,s_r) (i.e., left and right slopes), where $s_l=s[m-1,i]$, and $s_r=s[m,i]$ with

$$s[m,i]=y[m+1,i]-y[m,i]. \tag{1}$$

The allowed slope pairs for each model $B(1/2)$ through $B(2)$ are indicated in Fig. 1. The advancement probability is governed by the configuration of neighboring slopes and also by the parameter $p(=1-q)$.

The models' advancement rules are presented in terms of the probability of site $y[m,i]$ advancing by one unit during the current time step. The probability depends on the slope pair at that point and the parameter p, so it can be expressed as a matrix $\mathcal{P}_{B(M)}[s_l,s_r]$ which is a function of p. The probability matrix for each of the models considered here is presented in Tables I–IV.

Consider $B(1/2)$ in Table I. The slope pairs denoted by $(1/2,1/2)$ and $(-1/2,-1/2)$ represent superkinks which are responsible for the motion of the dislocation. They must advance in the presence of any applied stress. The rule for advancement of a segment $y[m,i]$ in either of these slope pairs is $y[m,i+1]=y[m,i]+1$. The segment $(-1/2,1/2)$ (''V'' shaped) represents the portion of the superkink in

TABLE I. This is the probability table for $B(1/2)$.

$\mathcal{P}_{B(1/2)}$	$-\frac{1}{2}$	$\frac{1}{2}$
$-\frac{1}{2}$	1	1
$\frac{1}{2}$	p	1

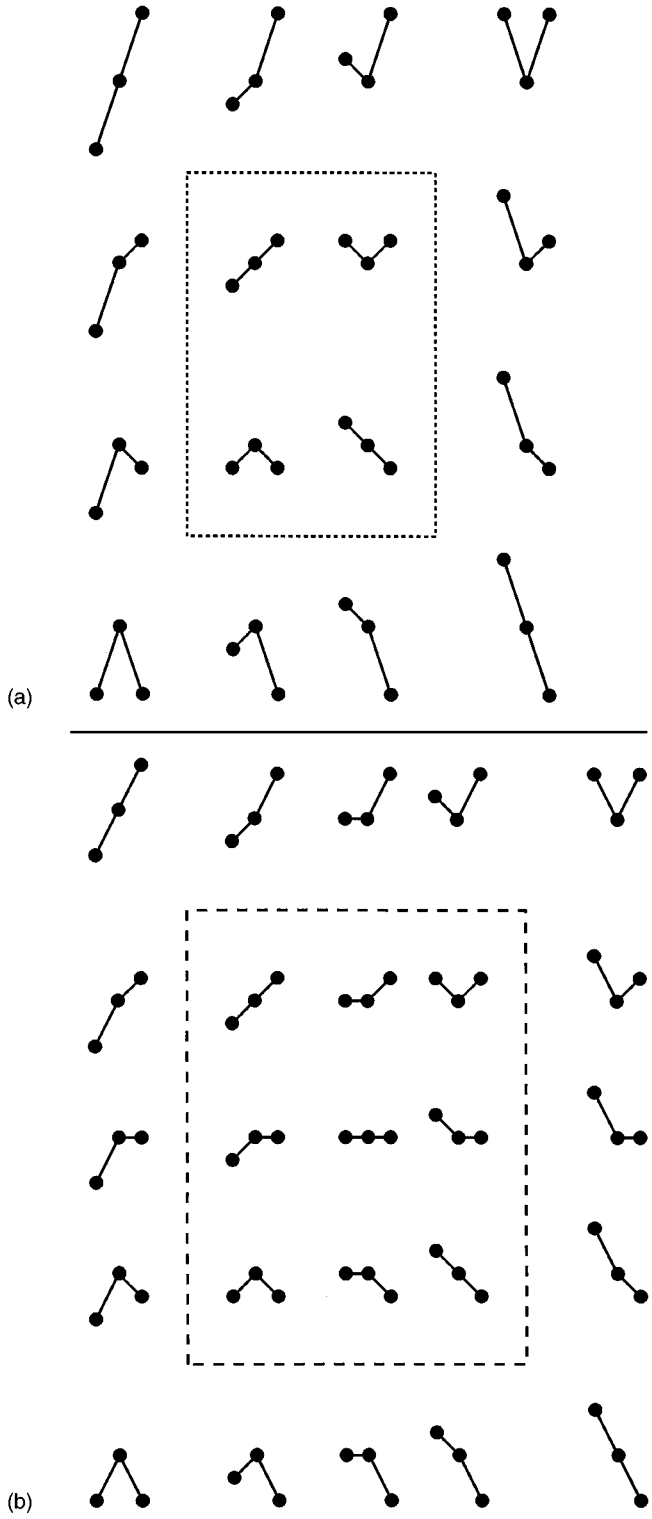

FIG. 1. The allowed slope pairs for each model $B(1/2)$ through $B(2)$. (a) The configurations for $B(3/2)$ are pictured; those for $B(1/2)$ are the subset in the dashed box. (b) The configurations for $B(2)$ are pictured; those for $B(1)$ are in the subset in the dashed box.

which the pinned (i.e., cross-slipped) points are being mobilized because of the stress due to the dislocation line tension. These points also advance one unit at every step. The only remaining type of slope pair is denoted by $(1/2,-1/2)$ (inverted ''V''). These configurations are potential sites for new cross-slip events. The advancement rule for these points is $y[m,i+1]=y[m,i]+1$ with probability p, and $y[m,i+1]=y[m,i]$ with probability $1-p$.

TABLE II. This is the probability table for $B(1)$.

$\mathcal{P}_{B(1)}$	-1	0	1
-1	1	1	1
0	p	ε	1
1	p	p	1

Table II contains the advancement probabilities for $B(1)$. The segments of type $(1,1)$ and $(-1,-1)$ represent superkinks, and their associated segments advance with probability one. The segments of type $(-1,0)$, $(-1,1)$, and $(0,1)$ represent slope pairs which will be depinned by the applied stress; these segments also advance with probability one. The segments of type $(1,-1)$, $(1,0)$, and $(0,-1)$ are potential points for cross slip to occur (or, conversely, spawning points for superkinks). The advancement probability for these segments is given by p. Finally, the segments of type $(0,0)$ represent the fully formed and locked Kear-Wilsdorf locks. These can be unlocked with the small, thermally activated rate ε.

Table III contains the advancement probabilities for $B(3/2)$. In this model the distinction between immobile and mobile superkinks is made. The mobile superkinks have the slope pairs $(3/2,3/2)$ and $(-3/2,-3/2)$, and these have advancement probabilities of one. The immobile superkinks have the slope pairs $(1/2,1/2)$ and $(-1/2,-1/2)$. Segments such as these are deemed to advance with probability ε corresponding to the possibility that their motion may be thermally activated. In addition, the segments $(-1/2,1/2)$ and $(1/2,-1/2)$ are mobile with a probability ε. The segments adjacent to superkinks will move according to the following rule. Those segments of type $(-3/2,s_r)$, where $s_r=-1/2$, $1/2$, or $3/2$, will advance with a probability of one because these segments represent the points in the dislocation at which a Kear-Wilsdorf lock is being dynamically annihilated. Similar arguments apply to the $(s_l,3/2)$ where $s_l=-3/2,-1/2,1/2$. Finally, because superkinks may beget superkinks with a probability p, the advancement probabilities for the remaining segment types are defined to be p.

Table IV displays the advancement probabilities for $B(2)$. These advancement probabilities are very similar to those employed in the prior model of Ref. 9. However, in contrast to the model of Ref. 9, the configurations which may spawn superkinks all do so with equal probability: No details reflecting the local curvature of the dislocation are included. While these details may be important to quantitative comparisons between experiment and theory, they obfuscate the

TABLE III. This is the probability table for $B(3/2)$.

$\mathcal{P}_{B(3/2)}$	$-\frac{3}{2}$	$-\frac{1}{2}$	$\frac{1}{2}$	$\frac{3}{2}$
$-\frac{3}{2}$	1	1	1	1
$-\frac{1}{2}$	p	ε	ε	1
$\frac{1}{2}$	p	ε	ε	1
$\frac{3}{2}$	p	p	p	1

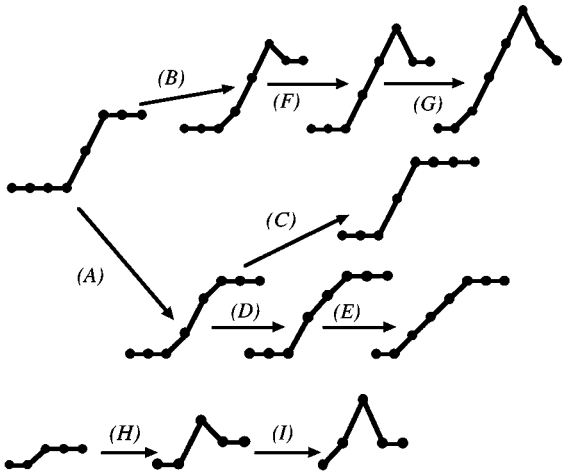

FIG. 2. Example pathways for a superkink in $B(2)$.

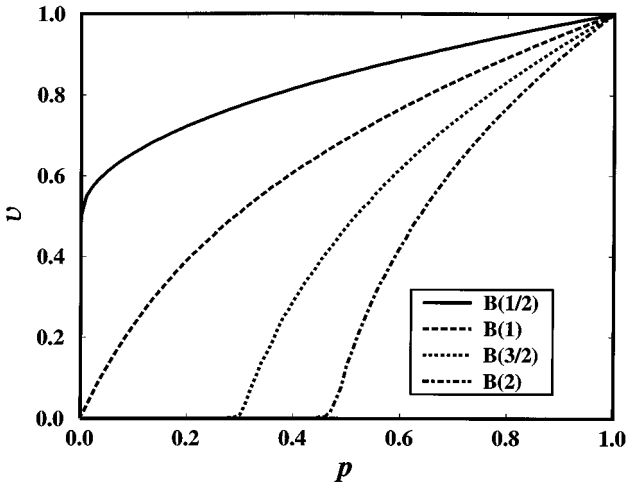

FIG. 3. The velocity vs p for $B(1/2)$ through $B(2)$.

scaling properties of the transition. The scaling properties of $B(2)$ (with $\varepsilon=0$) have been compared with those observed in the prior model, and no differences have been found.

This completes the specification of the dynamics of the models. The rules have been tailored to try to reproduce the motion of superkinks, formation of locks, and spawning of superkinks by other superkinks, all of which have been observed in a more detailed model of dislocation dynamics.[8]

Two choices of boundary conditions for the model are considered: (1) open boundary conditions and (2) periodic boundary conditions. For open boundary conditions, the ends of the dislocations, which correspond to the surface of the grain or single crystal, act as sinks for superkinks, and will influence the nature of the pinning-depinning transition. One natural boundary condition is to mimic the tendency of dislocations to intersect surfaces at a perpendicular. This ''zero-slope'' boundary condition is applied by requiring that the configurations on the ends of the dislocation are of the type $(s_l, s_r = -s_l)$. Another natural boundary condition is to impose periodic boundary conditions on the dislocation line. The results presented in this paper use the former type (open boundary), though we have compared these results to those with periodic boundary conditions and find that the general results do not appear to be sensitive to the choice.

Figure 2 displays possible pathways for the time evolution of a simple superkink configuration in $B(2)$. The path denoted by $(A)\rightarrow(D)\rightarrow(E)$ is a path by which the mobile superkink may become immobile. The path labeled $(A)\rightarrow(C)$ is the path by which the superkink moves to the left by one unit. The path labeled $(B)\rightarrow(F)\rightarrow(G)$ is a path by which the left-moving superkink may spawn an additional right-moving superkink. The path denoted by $(H)\rightarrow(I)$ is a path by which a pair of superkinks may be nucleated thermally from a pinned segment.

TABLE IV. This is the probability table for $B(2)$.

$\mathcal{P}_{B(2)}$	-2	-1	0	1	2
-2	1	1	1	1	1
-1	p	ε	ε	ε	1
0	p	ε	ε	ε	1
1	p	ε	ε	ε	1
2	p	p	p	p	1

The examples above indicate how in $B(2)$ superkinks act as sources for additional superkinks, as well as how a superkink may become immobile. This happens as well in $B(3/2)$ and $B(1)$. $B(1/2)$ is exceptional, however, in that superkinks are generated not by other superkinks, but instead by the particular slope-pair $(1/2,-1/2)$ (inverted ''V''). This property serves to simplify the dynamics of $B(1/2)$ which allows the exact solution to this model to be obtained, as outlined in Sec. III.

In metal plasticity, one is concerned with the strain accumulated through the motion of the dislocations. This strain is proportional to the total area swept out by the dislocations. Similarly, the strain rate is related to the areal velocity of the dislocations. The velocity of a single point $v[m,i]$ is $y[m,i+1]-y[m,i]$. The average velocity at step i, $v[i]$, is given by

$$v[i]=\frac{1}{L}\sum_{m=1}^{L} v[m,i], \tag{2}$$

where L is the number of segments in the dislocation. In the limit that $i\rightarrow\infty$, $v[i]$ fluctuates about a steady-state velocity, v_∞.

The statistically steady-state velocities are plotted in Fig. 3 for $B(1/2)-B(2)$ for the case in which $\varepsilon=0$. For $B(1/2)$, the dislocations' steady-state velocity is 1/2 for $p=0$ and saturates as $p\rightarrow 1$. Thus $B(1/2)$ exhibits only one state, which is mobile. Similarly, $B(1)$ describes dislocations mobile at all values of $p>0$. By contrast, $B(3/2)$ and $B(2)$ show two states: a pinned and unpinned state (or an immobile and a mobile state) separated by a critical value p_c.

By extensive numerical simulations of the stochastic equations embodied in Tables I–IV, we have explored the nature of the mobile and immobile states for dislocations of finite length. In particular, we find that the immobile state $(p<p_c)$ is degenerate, in that a large multiplicity of pinned configurations can be accessed here. If a pinned configuration is made mobile by releasing one of the pinned segments, the entire dislocation becomes active, with the mobile segments moving along the dislocation line, unzipping locked

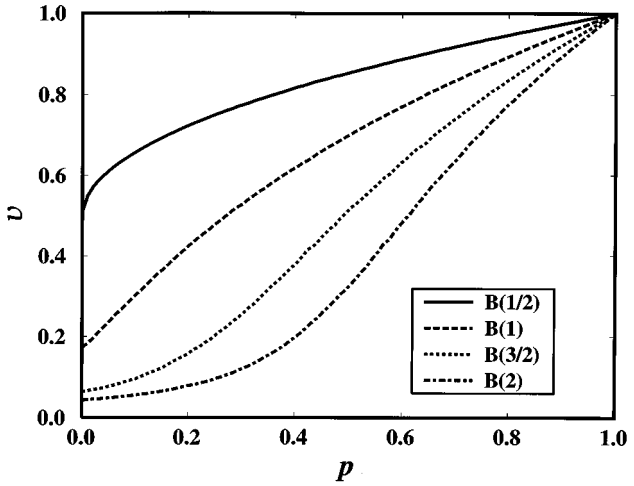

FIG. 4. The velocity vs p for $B(1/2)$ through $B(2)$ for $\varepsilon = 0.02$.

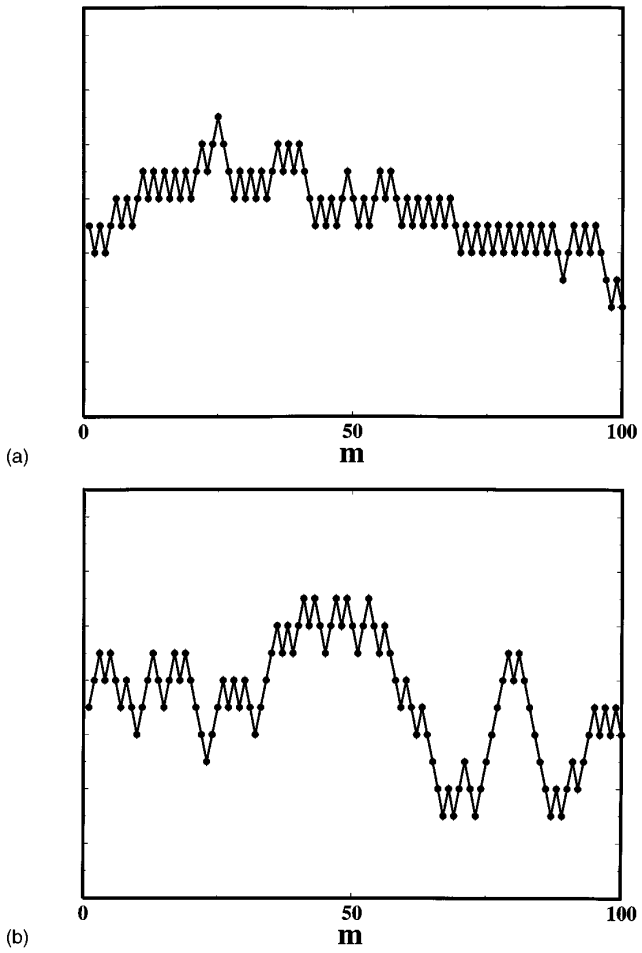

FIG. 5. Typical configurations for $B(1/2)$: (a) at small p, (b) at large p.

segments. The dislocation accelerates, then begins to slow as locking reoccurs until finally the entire dislocation becomes immobilized again. A similar relaxation occurs in the mobile state ($p > p_c$). In this case, a fluctuation away from the steady-state velocity gradually decays. Both below and above the critical point, the decay of fluctuations is characterized by a time scale which appears to diverge (except for finite-size effects) at the transition. We discuss the characteristic times in Sec. V.

We show in Fig. 4 the effect of finite ε on the steady-state velocities. Some rounding of the velocities occurs near the transition. Also, the pinned phases are no longer pinned, but take on a small velocity, due to the small rate (ε) at which locked configurations are unlocked. This small depinning removes the singular nature of the transition and gives a small mobility to the pinned phase. However, a vestige of the transition remains in the form of scaling behavior. We save a further discussion of the scaling behavior for Sec. V.

The behavior of this system is reminiscent of that expected for charge density waves[11] (in the strong-pinning limit), a system which has been argued to display critical behavior. It is argued below that the models studied here display critical behavior similar, though not identical to, that predicted for charge density waves. In particular, in the following sections we explore evidence of critical behavior in these models. In Sec. III, we present an analytical treatment of the simplest model, $B(1/2)$. Though $B(1/2)$ does not have a distinct pinned phase, we demonstrate that a ''trivial'' transition occurs precisely at $p = 0$. In Sec. IV, we explore numerical mean-field solutions for the more robust transitions seen in $B(3/2)$ and $B(2)$, each of which has two distinct phases. In the last section, we explore the scaling behavior.

III. ANALYTICAL MEAN-FIELD SOLUTION TO $B(1/2)$

The simplest model in the class is $B(1/2)$. Figure 3 shows that $B(1/2)$ displays no pinned phase and therefore no nontrivial pinning-depinning transition. However, as is demonstrated below, a transition appears precisely at $p = 0$. Also, one can make significant progress analytically when studying $B(1/2)$. Hence, $B(1/2)$ presents a convenient point from which one can begin to understand the behavior of the more complex models.

Typical steady-state configurations are presented in Fig. 5 for $p = 0.01$ and $p = 0.99$. For small p, the dominant feature is a ''picket fence'' interrupted occasionally by sloped superkinks. The picket fence moves with a velocity of 1/2. Occasionally (according to Table I) a spike in the picket fence will generate a pair of superkinks which travel apart. The presence of the superkinks raises the velocity above 1/2. At high p, the dislocation shows larger height-height variation, with a significant number of superkinks.

The evolution of a configuration similar to that of Fig. 5(a) is presented in Fig. 6. The state retains its qualitative character. The superkinks which are present move laterally. In Fig. 7, we plot the motion of the *superkinks* alone, which clearly illustrates the spontaneous creation of right- and left-traveling kink pairs which move to annihilate against each other. The overall forward motion of the dislocation is increased by the lateral motion of these superkinks: the forward velocity of the dislocation is linearly related to the density of kinks.

By contrast to the case for low p where the kink density is

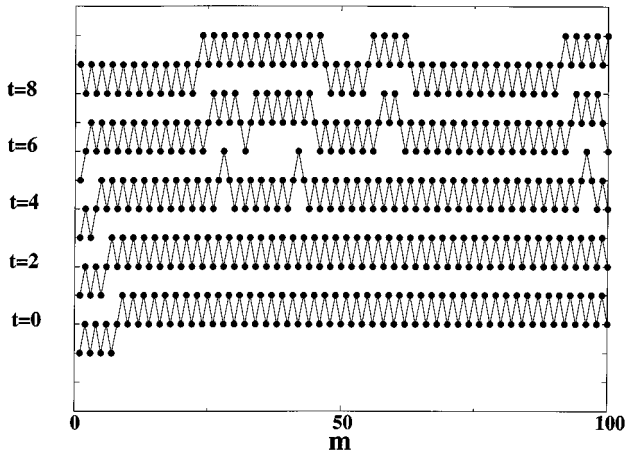

FIG. 6. Evolution of configuration shown in Fig. 5(a). Snapshots are taken at intervals of two time steps.

low, the configuration for high p (high kink density) moves forward largely unchanged.

Kinks are produced according to Table I by ''top'' (i.e., inverted-''V'') sites. A top site is one with neighboring slopes $(s_l, s_r) = (1/2, -1/2)$. When a top site moves forward (which it does with probability p), it generates a pair of superkinks. Thus for p near 1, nearly all top sites are generating near kink pairs. However, the presence of superkinks reduces the number of top sites, which slows the production of superkinks. This site blocking is the only form of correlation in the model. Otherwise, the generation of superkinks is completely random.

Thus the $B(1/2)$ model is quite simple: superkinks are produced at random in regions without superkinks and then move to annihilate with the next available kink moving in the opposite direction. In this sense, the $B(1/2)$ model is oversimplified in comparison to, say, $B(2)$, where only superkinks can spawn other superkinks. However, the simplicity makes $B(1/2)$ amenable to analytic solution. The lack of correlation among superkinks implies that a mean-field approximation will be reasonable. In fact, the statistical mean-field solution constructed in this section is the exact solution.[12]

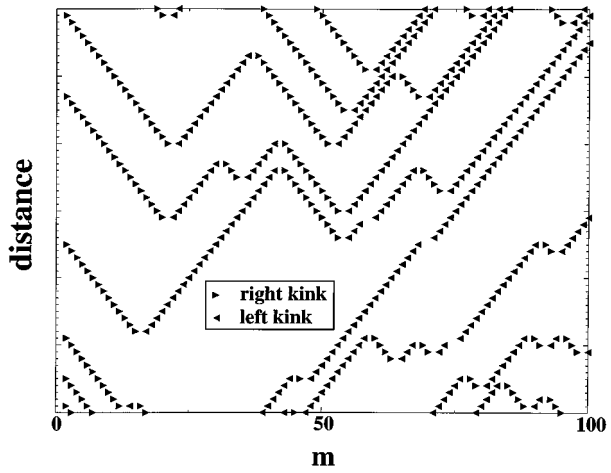

FIG. 7. Trajectories of superkinks in $B(1/2)$. Left-moving superkinks are plotted with left-pointing triangles and similarly for right-moving superkinks. Creation and annihilation events occur at the intersections of the lines.

As defined above, the distance along the slip direction of the mth node at ith time step is denoted by $y[m,i]$. The slope between neighboring nodes is constrained to have value $s[m,i] = \pm 1/2$. It is convenient to define topological charges which characterize the four possible slope pairs at each node:

$$\begin{aligned}
\hat{r}[m,i] &= (1/2 - s[m-1,i])(1/2 - s[m,i]), \\
\hat{l}[m,i] &= (1/2 + s[m-1,i])(1/2 + s[m,i]), \\
\hat{t}[m,i] &= (1/2 + s[m-1,i])(1/2 - s[m,i]), \\
\hat{b}[m,i] &= (1/2 - s[m-1,i])(1/2 + s[m,i]),
\end{aligned} \tag{3}$$

where $\hat{r}$ and $\hat{l}$ denote right- and left-moving superkinks, respectively, and $\hat{t}$ and $\hat{b}$ denote top and bottom sites, respectively. In each case, the charge of the site is either 0 or 1, depending on whether it fits the desired character.

From Table I, we see that all sites always move forward except top sites, which may cross slip and so lag behind.

The motion of the site m can be expressed as a stochastic, finite difference equation:[13]

$$y[m,i+1] - y[m,i] = \Delta y[m,i] = 1 + (p[m,i] - 1)\hat{t}[m,i], \tag{4}$$

where Δ is the time-step operator. In this equation, the process $p[m,i]$ is chosen randomly from 0 or 1 such that

$$\overline{p[m,i]} = p, \tag{5}$$

where the overbar indicates an average over the samples of the process p. Random numbers at different nodes and time steps are uncorrelated:

$$\overline{p[m,i]p[m',i']} = \delta_{m,m'}\delta_{i,i'}(p - p^2) + p^2. \tag{6}$$

These equations describe the motion of the dislocation completely, as prescribed by Table I.

Consider now the operation of averaging over the dislocation line: $\langle s[m,i] \rangle_m$ indicates an averaging of $s[m,i]$ over sites, so that it is the average slope along the dislocation. For example, the slope-slope correlation function at a given time step i is defined by an average over the length of the dislocation line:

$$P[n] = \langle s[m,i]s[m+n,i] \rangle_m = \frac{1}{L}\sum_{m=1}^{L} s[m,i]s[m+n,i]. \tag{7}$$

It is simple to prove that the nearest-neighbor correlation counts the number of superkinks:

$$P[1] = (1/2)\langle \hat{r}[m,i] + \hat{l}[m,i] \rangle_m - 1/4 \tag{8}$$

and that because the average slope of the infinite dislocation line must be zero, the number of right- and left-traveling superkinks are equal. Similarly, one can show that

$$P[1] = 1/4 - \langle \hat{t}[m,i] \rangle_m = 1/4 - \langle \hat{b}[m,i] \rangle_m \tag{9}$$

so that the concentration of the four charges is determined by one variable, which we define to be $x[i]=\langle \hat{r}[m,i]\rangle_m$.

The dislocation velocity is then given by

$$\begin{aligned} v[i] &= \frac{1}{L}\sum_{m=1}^{L} v[m,i] \\ &= \frac{1}{L}\sum_{m=1}^{L} \Delta y[m,i] \\ &= \frac{1}{L}\sum_{m=1}^{L} 1+(p[m,i]-1)\hat{t}[m,i]. \end{aligned} \tag{10}$$

Averaging the velocity over the random numbers, the statistically averaged dislocation velocity is then given by

$$\begin{aligned} \overline{v[i]} &= \overline{\langle v[m,i]\rangle_m} \\ &= (3+p)/4+(1-p)P[1] \\ &= (1+p)/2+(1-p)x[i], \end{aligned} \tag{11}$$

which shows that the velocity is linearly proportional to the density of kinks. To get an equation of motion for the statistically averaged dislocation velocity, we take the time step of $v[m,i]=1+(p[m,i]-1)\hat{t}[m,i]$, using the relation $\Delta(ab)=\Delta(a)b+a\Delta(b)+\Delta(a)\Delta(b)$, the definition of $\hat{t}$ in terms of the slopes s [Eq. (3)], the definition of the slopes s in terms of the heights y [Eq. (1)], and the equation of motion of the heights [Eq. (4)]. To obtain the statistical average over random pinning events, we average over the samples of the process p using its properties [Eqs. (5) and (6)]. Finally, we add up the sites along the length of the line to get the dislocation velocity:

$$\begin{aligned} \Delta v[i] &= (1-p)+4(1+3p)P[1]-8(1+p)P[2] \\ &\quad -4(1-p)P[3]+8(1-p)(T[1,3]-T[2,3]) \\ &\quad +16(1-p)Q[1,2,3], \end{aligned} \tag{12}$$

where $P[n]$ is the slope-slope (or ''pair'') correlation function from Eq. (7), $T[m,n]$ is the trio correlation $\langle s[0,i]s[m,i]s[n,i]\rangle_m$, and $Q[l,m,n]$ is the similar quartet correlation. In this way, the stochastic difference equation for L segments on the line is converted to a deterministic set of difference equations involving the statistical correlation functions.

The condition of steady state requires that the average of time derivatives of certain quantities vanish. For example, the requirement that the velocity be steady on average gives

$$\overline{\Delta v}=0, \tag{13}$$

which leads to

$$\begin{aligned} 0 &= (1-p)+4(1+3p)P[1]-8(1+p)P[2]-4(1-p)P[3] \\ &\quad +8(1-p)(T[1,3]-T[2,3])+16(1-p)Q[1,2,3]. \end{aligned} \tag{14}$$

This restriction on the correlation functions at steady state is exact. The same condition is obtained by applying the steady-state condition to any of the charges $\hat{t}$, $\hat{b}$, $\hat{r}$, or $\hat{l}$, because these charges involve products of nearest-neighbor slopes. Similar restrictions on more correlation functions are obtained by applying the steady-state condition to other quantities, such as a product of slope pairs which are not nearest neighbors, or products of three slopes, etc. Thus the steady-state condition gives rise to an infinite hierarchy of algebraic conditions on the correlation functions.

The mean-field solution begins with one noting that each slope pair (s_l,s_r) occurs with probability $\rho[s_l,s_r]=(1/4)+\alpha s_l s_r$, where $\alpha=(4x-1)$. (Note that $x\equiv\rho[1/2,1/2]$ by definition.) Joint probabilities are assumed to be products of the pair probabilities, so that the probability of the sequence $s1,s2,s3$ occurring is $\rho[s1,s2,s3]=\rho[s1,s2]\rho[s2,s3]$, etc. Then the mean-field second-nearest-neighbor pair correlation function $P_{\rm mf}[2]$, for example, is given by

$$P_{mf}[2]=Z^{-1}\sum_{\{s[m,i]\}} \rho[\{s[m,i]\}]s[0,i]s[2,i] \tag{15}$$

with

$$Z=\sum_{\{s[m,i]\}} \rho[\{s[m,i]\}] \tag{16}$$

and $\{s[m,i]\}$ denotes the set of all possible slope. The relevant correlation functions can be evaluated easily using transfer matrices,[14] to give

$$\underbrace{\langle s[0,i]s[j,i]s[k,i]s[l,i]\ldots s[p,i]\rangle}_{\text{n slopes}}{}_m = \begin{cases} (\frac{1}{2})^n(4x-1)^{(j-k+l-\ldots+p)} & , n \text{ even} \\ 0 & , n \text{ odd} \end{cases} \tag{17}$$

and so forth. (Note that it is assumed that $j\leq k\leq l\ldots\leq p$.)

Requiring that the mean-field correlation functions describe the system in steady state [Eq. (14)] gives a constraint on the kink density:

$$0=(-1+p)^2(1-2x)(p-4px-4x^2+4px^2)/2. \tag{18}$$

It is shown in Ref. 12 that the mean-field solution indeed satisfies all of the conditions for a steady-state solution, and is, therefore, the exact solution to the problem.

The solution to the steady-state equation for x gives the steady-state density of superkinks as a function of p:

$$x(p)=\langle \hat{r} \rangle = \frac{\sqrt{p}}{2(1+\sqrt{p})} \tag{19}$$

and the steady-state dislocation velocity as a function of p is

$$v_\infty(p)=\frac{(1+\sqrt{p})}{2}. \tag{20}$$

This form for the velocity fits the numerical results [Fig. 3 for $B(1/2)$] to within the accuracy of our numerical simulations.

It is now argued that this model displays critical behavior in the limit $p \to 0$.

Given the mean-field approximation, the slope-slope correlation function becomes

$$P[n]=\frac{(-1)^n}{4}\exp[n\ln(1-4x)]. \tag{21}$$

The correlation length, therefore, becomes

$$\xi=\frac{-1}{\ln(1-4x)}, \tag{22}$$

where x is the density of superkinks in steady state [Eq. (19)]. For small p, the density of superkinks $x \sim p^{1/2}$, and the correlation length $\xi \sim p^{-1/2}$. Hence the characteristic length in the problem diverges as the kink spawning probability approaches zero. This diverging correlation length is taken as evidence of a critical point at $p=0$.

The velocity fluctuations for $B(1/2)$ also indicate the presence of a critical point at $p=0$. Consider a case where the density of superkinks deviates from the steady-state value. The mean-field time dependence of the velocity is then given from the equation of motion for the velocity [Eq. (14)]. Using that equation and expanding the right-hand side to first order in $(v-v_\infty)$ gives

$$\Delta v = -2\sqrt{p}(1-\sqrt{p})(v-v_\infty), \tag{23}$$

which gives rise to an *exponential decay* with time constant $t_o=1/(2\sqrt{p})(1-\sqrt{p})$. Note that $t_o \to 1/(2\sqrt{p})$ as $p \to 0$. At precisely $p=0$ the relaxation equation for v becomes [to second order in $(v-v_\infty)$]

$$\Delta v = -2(v-v_\infty)^2, \tag{24}$$

which gives rise to an *algebraic decay*. The divergence of the exponential relaxation time and the emergence of an algebraic relaxation are taken as a sign of a depinning transition at precisely $p=0$. The exponent for the divergence of the relaxation time is $-1/2$.

If one assumes that the characteristic time governing the initial decay of the velocity-velocity correlation function is identical to that derived above, one can compare the mean-field result with numerical data obtained from the exact model. This comparison is shown in Fig. 8. The agreement between the mean-field result and the numerical result is excellent.

We have shown in this section through analytic means that even the simplest model in this class, $B(1/2)$, shows evidence of a dynamical phase transition, albeit a ''trivial'' one in the sense that no distinct pinned phase exists. In the next section, we will use a similar mean-field treatment for the more complex models of the class.

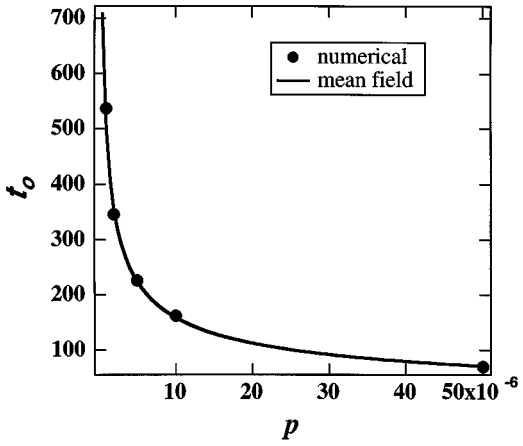

FIG. 8. Comparison of calculated and ''measured'' correlation times for $B(1/2)$.

IV. NUMERICAL MEAN-FIELD THEORY FOR $B(1)$, $B(3/2)$, AND $B(2)$

In the previous section, we showed evidence for a ''trivial'' dynamical phase transition in the simplest model of this class, $B(1/2)$. This solution was based on a mean-field treatment of the statistics, which is believed to be exact for this model. Qualitatively, one does not expect the mean-field solution to be exact for $B(M)$, with $M>1/2$. In $B(2)$, for example, superkinks spawn other superkinks [a process which does not happen in $B(1/2)$] so that spatial and temporal correlations between superkinks are more strongly evident. However, the mean field is nonetheless a good approximation to the exact numerical simulations, and therefore will serve in this section as a guide to the analysis. In addition, the mean-field solution may provide insight into behavior expected from more complicated experiments, e.g., internal friction measurements.

In slight contrast to $B(1/2)$, the equations of motion for the dislocation are calculated in terms of the average transition rate from a pair of type (s_l,s_r) to (s_l',s_r'). Consider a pair of slopes (s_l,s_r). This pair could evolve into a number of possible shapes at the next time step, depending on the slopes immediately to the left (s_λ) and right (s_ρ) and on the values of the random numbers (processes) in the equation of motion. Thus, specifying the sequence $(s_\lambda,s_l,s_r,s_\rho)$ determines completely the branching ratios of the central pair (s_l,s_r) into its various possible next states.

The transition rate for (s_l,s_r) to become (s_l',s_r') is

$$w[(s_l,s_r)\Rightarrow(s_l',s_r')]=\sum_{s_\lambda,s_\rho,s_\lambda',s_\rho'} f[s_\lambda,s_l,s_r,s_\rho] \times W[\{s_\lambda,(s_l,s_r),s_\rho\}\Rightarrow(s_l',s_r')]. \tag{25}$$

The function $f[s_\lambda,s_l,s_r,s_\rho]$ is the probability of finding the consecutive sequence of four slopes $(s_\lambda,s_l,s_r,s_\rho)$, given that the central pair is (s_l,s_r). $W[\{s_\lambda,(s_l,s_r),s_\rho\}$

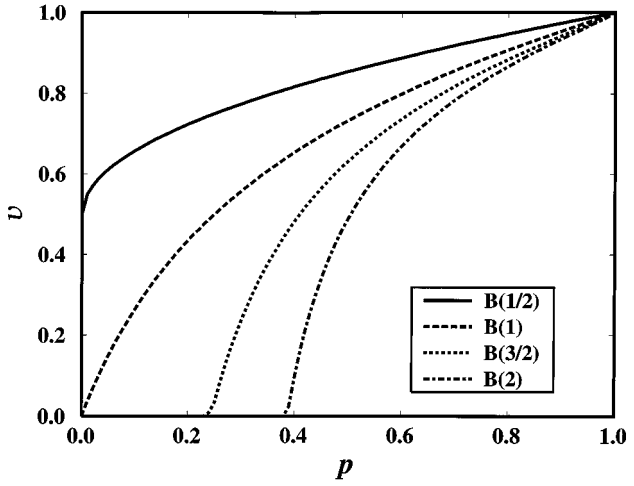

FIG. 9. Numerical mean-field solutions of the steady-state velocities for $B(1)$, $B(3/2)$, and $B(2)$.

$\Rightarrow(s_l',s_r')]$ is the transition rate for the pair of slopes (s_l,s_r), which are the central pair of a sequence of four slopes $(s_\lambda,s_l,s_r,s_\rho)$, to end up as the pair (s_l',s_r').

As with the $B(1/2)$ model, we make the mean-field approximation, where one neglects correlations between slope pairs; all configurations appear with frequency dictated only by the average probability of finding these configurations in the dislocation line. The function f is then approximated by

$$f[s_\lambda,s_l,s_r,s_\rho]=\frac{\rho[s_\lambda,s_l]}{\Sigma_{s_\lambda'}\rho[s_\lambda',s_l]}\frac{\rho[s_r,s_\rho]}{\Sigma_{s_\rho'}\rho[s_r,s_\rho']}. \quad (26)$$

The transition rates are calculated based on the advancement probabilities given in Sec. II. The results of these calculations, which are straightforward, but tedious, are then incorporated into a set of coupled, nonlinear equations governing the evolution of the probability distributions:

$$\Delta\rho[s_l,s_r]=\sum_{s_l',s_r'}\{\rho[s_l',s_r']w[(s_l',s_r')\Rightarrow(s_l,s_r)] - \rho[s_l,s_r]w[(s_l,s_r)\Rightarrow(s_l',s_r')]\}. \quad (27)$$

These deteriministic equations can then be solved numerically to determine various features of the dynamics governing dislocation motion.

In Fig. 9, the numerical, mean-field velocities for $B(1)$, $B(3/2)$, and $B(2)$ are presented. [The results for $B(1/2)$ are identical to those presented in the previous section.] The thermal depinning rate (ε) is 0, to compare to the numerical simulations of the exact equations which are plotted in Fig. 3. The mean-field solutions bear a great resemblance to the exact numerical results. In particular, $B(1)$ displays a transition at $p=0$, and $B(3/2)$ and $B(2)$ display a pinning-depinning transition at a nonzero value of $p=p_c$.

Using the mean-field equations, we explore the nature of the pinning-depinning transition. For example, one can construct a random population of slope pairs, and evolve the populations using mean-field equations of motion [Eq. (27)]. While for $B(1)$, one always arrives at a steady, mobile state, for $B(3/2)$ and $B(2)$, one arrives at a unique mobile steady

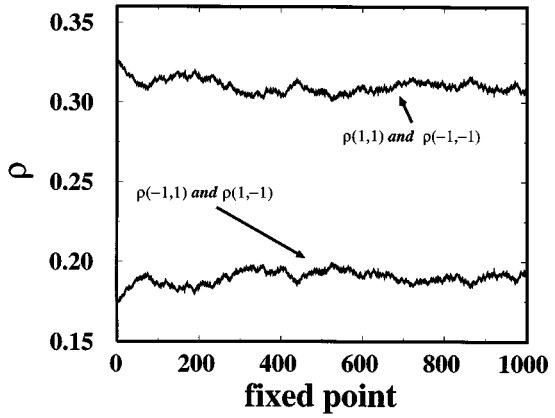

FIG. 10. The concentrations of various types of sites for exhausted configurations within the mean-field treatment. Each point on the curve is the result of one exhaustion event with $p=0.2$. The upper line is the probability that a spin pair is of the type $(-1,-1)$ and equals the probability that the spin pair is of type $(1,1)$. The lower curve is the probability of finding a pair of type $(-1,1)$ which is equal to the probability that a spin pair is of type $(1,-1)$. The equality of the respective pairs is determined by the initial conditions.

state for $p>p_c$. One also discovers that the immobile steady states $(p<p_c)$ are *not* unique. This is perfectly consistent with the exact solutions of the stochastic equations presented in Sec. II.

This behavior is displayed most clearly in the following thought experiment. Suppose one constructs a dislocation composed entirely of immobile superkinks (assuming that one is studying the models for $\varepsilon=0$). Then one can ''kick'' the dislocation by ''converting'' a single pinned slope pair to a mobile pair. In practice, this conversion is constructed to reflect accurately the symmetries imposed on the model by conservation of segment number, etc. The dislocation dynamics are allowed to evolve the system until a new fixed point is located. The final populations of slope pairs are recorded, and the procedure is repeated.

The results of such thought experiments are shown in Fig. 10. For advancement probabilities well below p_c, the slope-pair densities evolve toward what appears to be a statistically steady state. However, the statistically steady state appears to sample a significant number of distinct pinned configurations. Therefore, there is certainly more than one pinned state available to the system, even within the mean-field approximation. As the advancement probability is increased toward p_c, one still observes a spectrum of pinned states, but the ''width'' of this spectrum (in terms of the number of states available to the dislocation) is decreased markedly. Finally, for stresses above p_c, the steady state becomes truly unique, and the density of steady states becomes a delta function.

If one now sets $\varepsilon\neq0$, the results of this thought experiment change dramatically (Fig. 11). The dislocation is never pinned completely for any p. Within the mean-field approximation, then, in the finite temperature case, the sampling of phase space is altered substantially, and a particular state is selected, *even for those p much less than the zero-temperature critical probability,* p_c.

The mean-field approximation for $B(1)$, $B(3/2)$, and $B(2)$ is seen to be reasonably valid for these models, at least

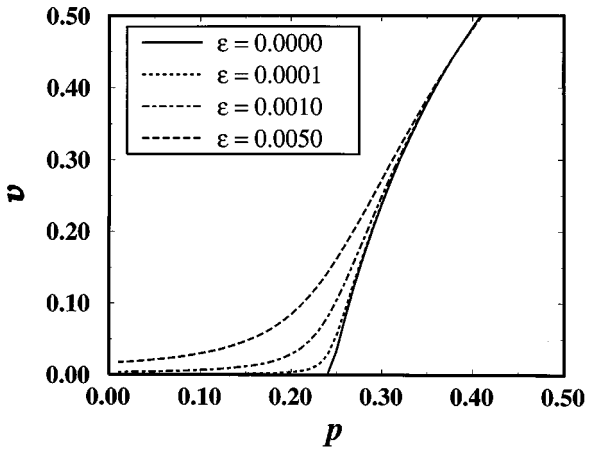

FIG. 11. $B(3/2)$ steady-state velocity (within the mean field), zero and finite ε.

in terms of the nature of the pinning-depinning transition and the velocity as a function of p. The mean-field solutions give some insight into the models. In the next section, we examine in detail the exact numerical solutions (for finite length) to the stochastic differential equations of motion.

V. NUMERICAL SCALING RESULTS

The models presented in Sec. II are based on stochastic, finite-difference equations of motion for the dislocation. In Secs. III and IV, we derived (from those stochastic equations) deterministic, mean-field equations of motion. In those sections, we saw that the mean-field approximations provided insight into the nature of the pinning-depinning transition for infinite systems. In this section, we obtain exact numerical results from the original stochastic equations for systems of finite size. Results are presented for $B(3/2)$ and $B(2)$. At zero temperature, $B(3/2)$ and $B(2)$ display a pinning-depinning transition at a nonzero value of p_c. The zero-temperature scaling properties of the transition are investigated for $B(3/2)$, and found to be consistent with the properties deduced in an earlier study of a model very similar to $B(2)$.[9] At finite temperature, the models no longer display a pinned phase. However, it is demonstrated that one can use the remaining vestige of the pinning-depinning transition to deduce critical exponents.

A. Scaling at zero temperature

Consider first the ''zero-temperature'' behavior of $B(3/2)$ (i.e., $\varepsilon=0$ in Table III). As stated above, in this model there are two *types* of states: a pinned state, in which the steady-state dislocation is immobile, and an unpinned state, in which the steady-state dislocation is mobile (in an infinite system). These two phases are delineated by a critical probability, p_c.

In the mobile phase ($p>p_c$), one expects that as $p\to p_c$, the velocity approaches zero as

$$v_\infty(p)\sim(p-p_c)^{\nu}, \tag{28}$$

based on an analogy with the electric field driving a charge density wave. A similar behavior is found for $B(1/2)$ [except that the left-hand side of Eq. (28) must be replaced by $v_\infty(p)-\frac{1}{2}$], and $\nu=\frac{1}{2}$. Similarly, one expects the characteristic time governing the velocity fluctuations to diverge according to

$$t_o\sim(p-p_c)^{-\phi'}. \tag{29}$$

For $p<p_c$ and $\varepsilon=0$ there are *many* pinned states. Even though all dislocations eventually become immobilized in this regime, their relaxation dynamics can be studied by giving an immobilized dislocation a small ''kick.'' Dislocations mobilized this way will move for some time, and then become immobile once again. It is expected that the characteristic time for this relaxation also diverges near the critical point as

$$t_o\sim(p_c-p)^{-\phi}. \tag{30}$$

It is not clear *a priori* that $\phi=\phi'$; however, the scaling analysis presented below suggests that the equality holds.

It is difficult to extract the exponents directly from the numerical calculations at zero temperature, due to finite-size effects. For example, in a dislocation of finite length, there is a small probability that a dislocation will become pinned, even in the mobile regime ($p>p_c$). The scaling behavior is more easily investigated at finite temperature (i.e., finite ε). The finite-temperature results are then combined with algebraic relations between exponents to deduce the zero-temperature behavior. This will be discussed in the next subsection.

At a critical point, one expects to observe scaling.[15] When an immobile dislocation is mobilized, as above, by a small kick, it will sweep at an area a before exhausting at a time t. This process is repeated, until a distribution of events can be accumulated. The distribution $n(a,t)dadt$ is defined to be the number of dislocations which sweep out an area between a and $a+da$ before exhausting at a time between t and $t+dt$. In Refs. 8 and 9, it was argued that near p_c, this distribution becomes a homogeneous function of its arguments:

$$\lambda n(a,t)=n(\lambda^{\alpha}a,\lambda^{\delta}t). \tag{31}$$

It is straightforward to demonstrate this scaling behavior even at zero temperature. Figure 12 shows the results for $B(3/2)$, where the values $\alpha=-1/2$ and $\delta=-1/3$ have been used. [These are the exponents deduced from earlier study of a model very similar to $B(2)$.[9] The data collapse suggests these exponents are good estimates for $B(3/2)$ as well.]

In addition, several other quantities related to $n(a,t)$ are expected to scale. For example, the average areal velocity at time t of a dislocation destined to become immobile at a time t', defined to be $v(t,t')$ is expected to scale according to

$$v(t,t')=t'^{\eta}g(t/t'). \tag{32}$$

One can show that $\eta=1/2$ for the choices of α and δ given above. This scaling form is also tested in Fig. 12 with $\eta=0.52$. In addition, given the values of α and δ, one expects the average area swept out by a dislocation destined to exhaust at time t, defined to be $\bar{a}(t)$, to scale according to

$$\bar{a}(t)\sim t^{\alpha/\delta}. \tag{33}$$

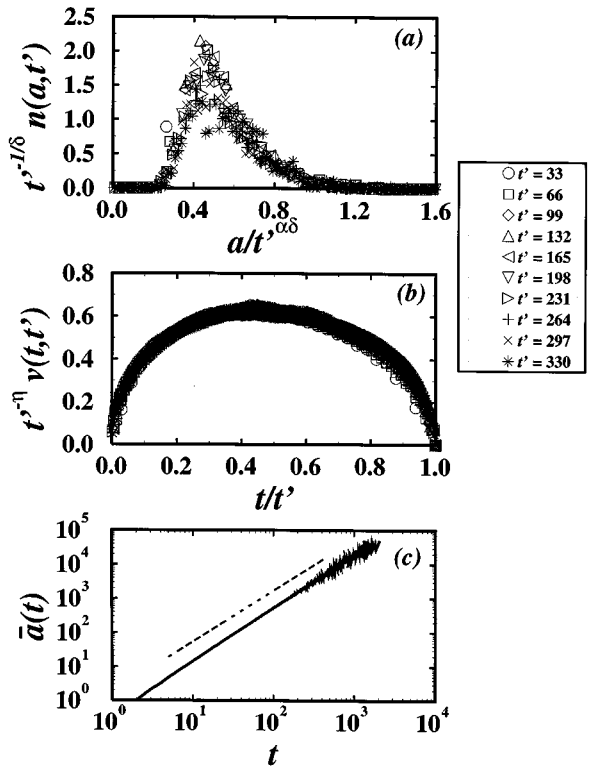

FIG. 12. Scaling behavior of $B(3/2)$ for $\varepsilon=0$. Panel (a) displays the scaling of $n(a,t)$ with $\alpha=-\frac{1}{2}$ and $\delta=-\frac{1}{3}$. Panel (b) displays the scaling of $v(t,t')$ with $\eta=0.52$. Panel (c) displays the observed behavior of $\overline{a(t)}$. The dashed line in panel (c) displays the expected $t^{3/2}$ dependence.

This behavior is also consistent with the choice $\alpha=-1/2$ and $\delta=-1/3$, as demonstrated in Fig. 12.

In summary, there is good numerical evidence for the criticality and scaling behavior. Table V summarizes the expected zero- (and finite-) temperature scaling behaviors.

B. Scaling at nonzero temperature

At finite temperatures, the transition between pinned and unpinned phases is eliminated: A dislocation is mobile even for probabilities $p<p_c$. However, this does not mean that the scaling behavior present in the models for $\varepsilon=0$ is absent completely from the finite ε solution. In fact, it is demonstrated here that introduction of a finite value of ε has an effect similar to the introduction of temperature into the Fukuyama-Lee-Rice model[16,17] of charge density waves.[11,18] By analogy with those studies, the following scaling form is conjectured to hold for v_∞ as a function of p:

$$v_\infty(p,\varepsilon)=\varepsilon^{\beta} f((p-p_c)/\varepsilon^{\gamma}). \tag{34}$$

This expression is based on the fact that the introduction of temperature (i.e., finite ε) results in an additional time scale characterizing the dislocation dynamics. At the critical point, this time scale must be the only time scale in the problem, for $t_o\to\infty$. Therefore, near p_c, only the ratio of $(p-p_c)/\varepsilon^{\gamma}$ determines the behavior of the dislocation, barring the effects of finite size. (In fact, this argument is similar to that used for analyzing finite-size effects except for the fact that the additional length scale stems from the thermally activated step, and not the size of the system.)

Because the $\varepsilon\to 0$ limit of $v_\infty(p,\varepsilon)$ is $v_\infty(p)$, the scaling hypothesis requires that the critical exponents satisfy

$$\beta-\gamma\nu=0. \tag{35}$$

This relation is used to calculate the zero-ε exponent ν from calculations done at finite ε.

This type of argument can be extended further to aid in analysis of the characteristic time scale for the velocity fluctuations. It is conjectured here that for the finite-temperature case,

$$t_o(p,\varepsilon)=\varepsilon^{-\zeta} h((p-p_c)/\varepsilon^{\gamma}). \tag{36}$$

To correspond to $t_o(p)$ in the zero-ε limit, the critical exponents must satisfy

$$\zeta-\gamma\phi=0. \tag{37}$$

We now test the scaling hypotheses for the velocity and characteristic time [Eqs. (34) and (36)]. The characteristic time is estimated from the velocity autocorrelation function. A dislocation with $L=10^4$ is initialized to a symmetric state. (For example, for $B(2)$ the dislocation is initialized with $y[m,0]=0$ for all m.) The system is run for 10^5 steps to allow the system to approach its statistically steady state. The velocity is then recorded for $T=4\times10^5$ steps, and v_∞ is calculated as

$$v_\infty=\frac{1}{T}\sum_{i=1}^{T} v[i]. \tag{38}$$

The velocity-velocity correlation function $\tilde{g}(n)$ is then estimated according to

$$\tilde{g}(n)=\frac{1}{N}\sum_{i=1}^{N}(v[i+n]-v_\infty)(v[i]-v_\infty), \tag{39}$$

TABLE V. Some scaling forms and *estimates* for exponents.

	$\varepsilon=0$ $(T=0)$	$\varepsilon>0$ $(T>0)$	Exponents
Velocity	$v_\infty(p)\sim(p-p_c)^{\nu}$	$v_\infty(p,\varepsilon)=\varepsilon^{\beta} f((p-p_c)/\varepsilon^{\gamma})$	$\beta=1/3$ $\gamma=1/3$ $\nu(=\beta/\gamma)=1$
Characteristic time	$t_o(p)\sim\lvert p-p_c\rvert^{-\phi}$	$t_o(p,\varepsilon)=\varepsilon^{-\zeta} h((p-p_c)/\varepsilon^{\gamma})$	$\zeta=2/3$ $\phi(=\zeta/\gamma)=2$

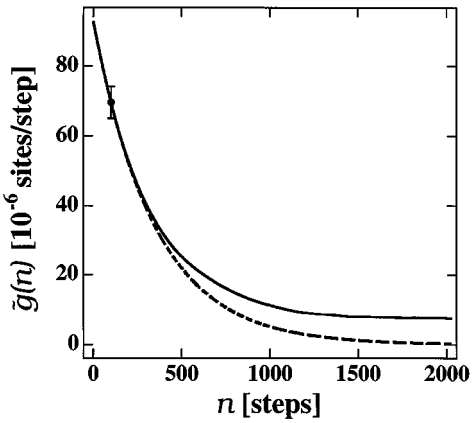

FIG. 13. Velocity autocorrelation function as ''measured'' using numerical simulations. The solid line is the numerical value estimated from 400 000 data points, and the dashed line is a fit to the data. The error bar indicates the statistical error.

where the value N depends on the number of points available for averaging. The characteristic time is estimated by fitting the ''early time'' portion of $\tilde{g}(n)$ to an exponential form

$$\tilde{g}(n)=\tilde{g}(0)\exp(-n/t_o), \tag{40}$$

where ''early time'' is defined to be $0\leq n\lesssim t_o/3$. The values so obtained are then used to verify the conjectured scaling forms above. Figure 13 contains an example of the correlation function so obtained, and the corresponding fit. The error bars in Fig. 13 represent a statistical estimate of the error. Note that the disagreement at long times between the fitted curve and the numerical data stems from the error in the numerical estimate of v_∞.

It is simplest to determine p_c from the scaling form for t_o [Eq. (36)]. One expects a peak in this distribution to appear at $p=p_c$, for sufficiently small ε. (One must be careful not to include ε so small that finite-size effects are evident.) This expectation is validated by the results for $B(3/2)$, which show a peak near $p=0.30$. Hence in constructing the scaling plot for $t_o(p,\varepsilon)$, the critical probability is chosen to be $p_c=0.30$. Figure 14 displays the scaled curves using the estimated values of the exponents $\zeta=0.63$ and $\gamma=0.32$. The data collapse for a range of ε varying over slightly more than one decade is excellent. For ε too large, the scaled data do not fall on the scaled curve. For $\varepsilon\lesssim 1/L$, the curves also do not fall on the scaled curve due most likely to the finite size of the dislocation.

The data collapse in Fig. 14 suggests that the scaling conjecture of Eq. (36) is a good one. The fact that the collapse persists through the zero-ε critical probability suggests that $\phi=\phi'$, though statistical noise precludes a definitive statement. The data collapse, when combined with the scaling form Eq. (37), allows an estimate of $\phi=1.9$.

A similar behavior is observed for $B(2)$, as is displayed also in Fig. 14. The critical exponents for this model agree, to within numerical accuracy, with those of $B(3/2)$. The critical probability is estimated to be $p_c=0.47$.

Having determined p_c through the analysis of the correlation time, it is now possible to test Eq. (34) for the scaling of the velocity. The above analysis has already established

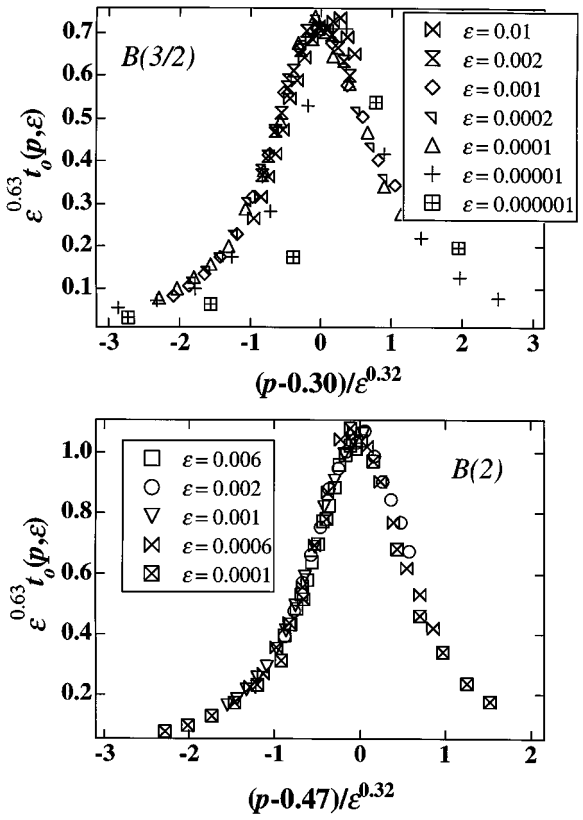

FIG. 14. Characteristic time data for $B(3/2)$ and $B(2)$.

that $\gamma\approx 0.32$, hence the only exponent remaining to be determined is β. This exponent can be estimated from a plot of $v(p_c,\varepsilon)$.

The results for $B(3/2)$ and $B(2)$ are presented in Fig. 15. The data collapse, obtained with $\beta=0.32$, verifies the proposed scaling form. This result, coupled with Eq. (35), implies that $\nu=1.0$. Hence the dislocation velocity is estimated to be a linear function of $p-p_c$ near the critical point.

VI. DISCUSSION

It has been argued in prior work that the total exhaustion of the motion of the dislocation is responsible for the observed anomalous hardening rates.[2] In fact, stress relaxation experiments performed by Bonneville and Martin indicate that even during the short duration of their relaxations, the mobile dislocation density is changing.[19] However, the current work, which indicates that inclusion of thermally assisted depinnning eliminates the existence of a pinned phase, requires a reanalysis of the proposed hardening mechanism. While the precise resolution of this issue awaits further study, some arguments are presented here.

In a truly infinite system at finite temperature, the dislocations never completely exhaust their motion. However, in a dislocation of finite length, which necessarily contains a finite number of superkinks, it is possible for the dislocation to be driven to a state in which the time for thermally assisted depinning initiation of dislocation motion, which is governed by the thermal bowing of immobile superkinks,[7] is much longer than the time scales associated with the experiment. For all practical purposes, then, this dislocation is pinned, and contributes to the observed hardening. Note that

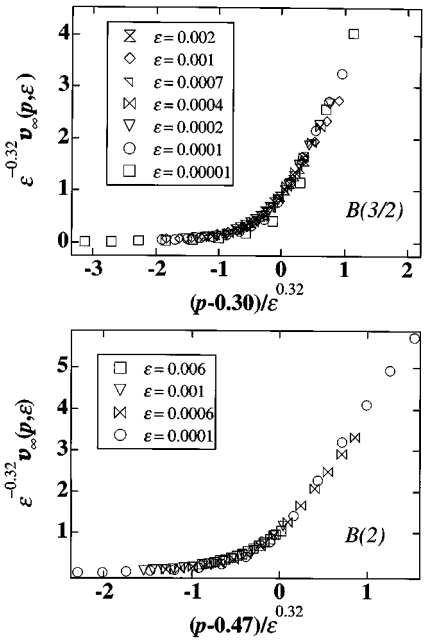

FIG. 15. The scaled velocity plots for $B(3/2)$ and $B(2)$.

the models of the class considered here could be modified to allow for several thermal depinning rates (configuration dependent) and the effects of these rates on the observed hardening determined.

In this picture, then, hardening is related intimately to the length of the dislocations. Therefore, one might expect *significant finite-size effects* (e.g., grain-size, etc.) in the hardening properties of these compounds. The authors are not aware of experiments designed to explore such dependence directly, but suggest that such experiments may prove fruitful.

VII. CONCLUSIONS

In conclusion, a set of models mimicking superdislocation motion in the $L1_2$ compounds displaying the yield strength anomaly are introduced and studied. The models include both dynamic and thermal annihilation of the Kear-Wilsdorf locks.

The most simple version of the model, $B(1/2)$ can be solved exactly. This exact solution, given in terms of an advancement probability, p, indicates the existence of a critical point at $p=0$. The exponents for this critical point are evaluated exactly.

For more complicated versions of the model, one can no longer obtain easily the exact solution. Instead, these models are studied within a mean-field approximation and through exact numerical techniques. For $B(3/2)$ and $B(2)$, the zero-temperature (i.e., no thermal annihilation of Kear-Wilsdorf locks) mean-field solution indicates the existence of a nonzero value of the advancement probability $p=p_c$ below which all superdislocations eventually become pinned. For $p>p_c$, an infinite dislocation remains mobile for all time. In addition, the mean-field solution suggests that there is a broad spectrum of accessible configurations for the super dislocations as long as $p<p_c$, but that for $p>p_c$, the dynamics select a particular configuration as the mobile one. In addition, the spectrum of accessible states appears to narrow continuously as one approaches p_c from below.

The inclusion of thermal annihilation of the Kear-Wilsdorf locks alters significantly the manner in which configuration space is sampled. Within the mean-field solution, the dislocation assumes a particular (p- and ε-dependent) mobile configuration for all values of p. Correspondingly, the pinning-depinning transition moves to $p=0$.

The mean-field solution suggests that study of the exact solution numerically is warranted. It is verified that the models studied here display a critical behavior similar to that proposed for a prior model of flow. In particular, it is found that various quantities related to mechanical properties should scale for $p\approx p_c$.

It is also noted that for $\varepsilon\neq 0$, that the critical point at p_c is no longer present. However, remnants of the scaling behavior associated with that critical point that are present for small ε allow one to develop a scaling analysis to determine critical exponents associated with the $\varepsilon=0$ critical point. In particular, it is argued, based on an analysis of the velocity-velocity correlation function, that the characteristic time, t_o, scales as $|p-p_c|^{\phi}$ with $\phi=1.9$. It is also argued that the velocity as a function of p scales in a fashion similar to that proposed by Middleton for charge density waves.

ACKNOWLEDGMENTS

The authors began this work when both were at Sandia National Labs in California, and acknowledge support there under Contract No. DE-AC04-94AL85000 from Department of Energy, Office of Basic Energy Sciences. M.S.D. also acknowledges support from the National Science Foundation under Grant No. 95-10259, and D.C.C. support from the Director, Office of Energy Research, Office of Basic Energy Sciences, Materials Sciences Division of the U.S. Department of Energy under Contract No. DE-AC03-76SF00098.

[1] V. Paidar, D. P. Pope, and V. Vitek, Acta Metall. **32**, 435 (1984).
[2] M. J. Mills and D. C. Chrzan, Acta Metall. Mater. **40**, 3051 (1992).
[3] B. H. Kear and H. G. F. Wilsdorf, Trans. TMS-AIME **224**, 382 (1962).
[4] M. J. Mills, N. Baluc, and H. P. Karnthaler, in *High Temperature Ordered Intermetallic Alloys III*, edited by C. T. Liu *et al.*, MRS Symposia Proceedings No. 133 (Materials Research Society, Pittsburgh, 1989), p. 203.
[5] Y. Q. Sun and P. M. Hazzledine, Philos. Mag. A **58**, 603 (1988).
[6] P. Veyssière, in *High Temperature Ordered Intermetallic Alloys III* (Ref. 4), p. 175.
[7] P. B. Hirsch, Philos. Mag. A **65**, 569 (1991).
[8] D. C. Chrzan and M. J. Mills, Phys. Rev. Lett. **69**, 2795 (1992).

[9] D. C. Chrzan and M. J. Mills, Phys. Rev. B **50**, 30 (1994).
[10] D. C. Chrzan and M. J. Mills, Dislocat. Solids (to be published).
[11] D. S. Fisher, Phys. Rev. B **31**, 1396 (1985).
[12] D. Marfatia and M. S. Daw (unpublished).
[13] R. Kubo, M. Toda, and N. Hashitsume, *Statistical Physics II: Nonequilibrium Statistical Mechanics*, Springer Series in Solid-State Sciences Vol. 31 (Springer-Verlag, New York, 1983).
[14] N. Goldenfeld, *Lectures on Phase Transitions and the Renormalization Group*, Vol. 85 of *Frontiers in Physics* (Addison-Wesley, New York, 1992).
[15] S. Ma, *Modern Theory of Critical Phenomena*, *Frontiers in Physics* (W. A. Benjamin, Inc., Reading, 1976).
[16] H. Fukuyama and P. A. Lee, Phys. Rev. B **17**, 535 (1978).
[17] P. A. Lee and T. M. Rice, Phys. Rev. B **19**, 3970 (1979).
[18] A. A. Middleton, Phys. Rev. Lett. **68**, 670 (1992).
[19] J. Bonneville and J. L. Martin (private communication).